HHS Public Access

Author manuscript

Biomed Pharmacother. Author manuscript; available in PMC 2017 August 11.

Published in final edited form as:

Biomed Pharmacother. 2017 May ; 89: 268–275. doi:10.1016/j.biopha.2017.01.144.

Synthesis, characterization and radiolabeling of polymeric nano-micelles as a platform for tumor delivering

Caroline Mari Ramos Oda[a], **Renata Salgado Fernandes**[a], **Sávia Caldeira de Araújo Lopes**[a], **Mônica Cristina de Oliveira**[a], **Valbert Nascimento Cardoso**[b], **Daniel Moreira Santos**[c], **Adriano Monteiro de Castro Pimenta**[c], **Angelo Malachias**[d], **Rogério Paniago**[d], **Danyelle M. Townsend**[e], **Patrick M. Colletti**[f], **Domenico Rubello**[g,*], **Ricardo José Alves**[a], **André Luís Branco de Barros**[b], and **Elaine Amaral Leite**[a,*]

[a]Department of Pharmaceutical Products, Faculty of Pharmacy, Universidade Federal de Minas Gerais, 31270-901 Belo Horizonte, Minas Gerais, Brazil

[b]Department of Clinical and Toxicological Analyses, Faculty of Pharmacy, Universidade Federal de Minas Gerais, 31270-901 Belo Horizonte, Minas Gerais, Brazil

[c]Department of Biochemistry and Imunology, Biological Science Institute, Universidade Federal de Minas Gerais, 31270-901 Belo Horizonte, Minas Gerais, Brazil

[d]Department of Physics, Exact Sciences Institute, Universidade Federal de Minas Gerais, 31270-901 Belo Horizonte, Minas Gerais, Brazil

[e]Department of Drug Discovery and Pharmaceutical Sciences, Medical University of South Carolina, United States

[f]Department of Nuclear Medicine, University of Southern California, Los Angeles, CA, United States

[g]Department of Nuclear Medicine, Imaging and Clinical Pathology, Santa Maria della Misericordia Hospital, Rovigo, Italy

Abstract

The use of nanoparticles for diagnostic approaches leads to higher accumulation in the targeting tissue promoting a better signal-to-noise ratio and consequently, early tumor detection through scintigraphic techniques. Such approaches have inherent advantages, including the possibility of association with a variety of gamma-emitting radionuclides available, among them, Tecnethium–99 m (^{99m}Tc). ^{99m}Tc is readily conjugated with nanoparticles using chelating agents, such as diethylenetriaminepentaacetic acid (DTPA). Leveraging this approach, we synthesized polymeric micelles (PM) consisting of 1,2-distearoyl-*sn*-glycero-3-phosphoethanolamine-*N*-[methoxy(polyethyleneglycol)-2000] (DSPE-mPEG$_{2000}$) functionalized with DTPA for radiolabeling with ^{99m}Tc. Micelles made up of DSPE-mPEG$_{2000}$ and DSPE-PEG$_{2000}$-DTPA had a mean diameter of ~10 nm, as measured by DLS and SAXS techniques, and a zeta potential of −2.7 ± 1.1 mV. Radiolabeled micelles exhibited high radiochemical yields and stability. In vivo assays

*Corresponding authors. domenico.rubello@libero.it, domenico.rubello@aulss5.veneto.it (D. Rubello), elaineleite@ufmg.br, leite_elaine@hotmail.com (E.A. Leite).

Conflict of interests: None

indicated long blood circulation time (456.3 min). High uptake in liver, spleen and kidneys was observed in the biodistribution and imaging studies on healthy and tumor-bearing mice. In addition, a high tumor-to-muscle ratio was detected, which increased over time, showing accumulation of the PM in the tumor region. These findings indicate that this system is a promising platform for simultaneous delivery of therapeutic agents and diagnostic probes.

Keywords

Polymeric micelles; Synthesis; Characterization; Radiolabeling; Platform for tumor delivering

1. Introduction

Over the last decades, nanoparticle based delivery platforms have attracted much attention due to their ability to selectively deliver drugs and/or imaging probes into tumors [1]. Many studies have reported significant advances in diagnostic applications [2–5]. Advantages of using radiolabeled nanoparticles for diagnostic approaches include higher accumulation in the targeting tissue, which in turn implies a better signal-to-noise ratio over standard scintigraphic detection methods. This technology might allow early tumor diagnosis that is essential for increasing overall patient survival [7].

Among the different types of nanostructured carriers, polymeric micelles (PM) have prominent characteristics, such as narrow size distribution, morphology, and surface properties that favor their accumulation in the tumor area [8]. PMs are globular nanostructures (with diameters ranging from 5 to 100 nm) formed by amphiphilic copolymers with lipophilic core showing a critical micellar concentration (CMC) ranging from 10^{-5} to 10^{-7} mol L^{-1}. In addition, PMs are proving to be versatile structures that allow high payloads of a myriad of molecules [9,10].

In this context, 1,2-distearoyl-*sn*-glycero-3-phosphoethanolamine-*N*-[methoxy(polyethyleneglycol)-2000] (DSPE-mPEG$_{2000}$) has been used to prepare PM [11,12]. Polyethyleneglycol (PEG) is a hydrophilic polymer, biocompatible and biodegradable, largely used for increasing blood circulation time of nanoparticles [13,14]. Additionally, the presence of a phospholipid, acting as the hydrophobic block, improves micelles stability due to the presence of two fatty acid chains that increases the number of hydrophobic interactions in this region [15]. Furthermore, DSPE-PEG$_{2000}$ allows the introduction of imaging probes by adding chelating agents on the PEG extremity [9,15]. This might be particularly advantageous since the simultaneous delivery of therapeutic agents and diagnostic probes leads to a theranostic platform that allows integrating tumor visualization and treatment into a single system.

Among diagnostic imaging approaches, scintigraphic techniques have significant importance due to their high sensitivity, which permits identification of molecular changes in the targeting tissue allowing earlier diagnosis [16–18]. One of the most common radioisotopes used in planar scintigraphic images and Single Photon Emission Computed Tomography (SPECT) is the technetium–99 m (^{99m}Tc). ^{99m}Tc has been widely used due to its nuclear properties, including the gamma energy of 140 keV, easy access through a molybdenum-99/

technetium–99 m generator, and half-life of 6.02 h [19–21]. Furthermore, ^{99m}Tc can be easily and stably complexed with chelating agents, such as diethylenetriaminepentaacetic acid (DTPA), for imaging purposes [22]. Our research group previously demonstrated the ability of ^{99m}Tc atoms to be complex with DTPA immobilized on the surface of silica nanoparticles. [2]

In this context, the aim of this study was to evaluate the ^{99m}Tc-PM as a potential platform for tumor delivery. To achieve this goal, DSPE-PEG$_{2000}$-DTPA was synthesized and characterized by ultraviolet (UV) spectroscopy, Fourier transform infrared spectroscopy (FTIR), and mass spectrometry (MS). Then, PMs were prepared, characterized by dynamic light scattering (DLS), Zeta potential and Small Angle X-ray Scattering (SAXS), and subsequently radiolabeled with ^{99m}Tc. Blood circulation time was determined in healthy mice, while biodistribution and scintigraphic images were conducted in healthy and tumor-bearing mice.

2. Experimental methods

2.1. Materials

1,2-distearoyl-sn-glycero-3-phosphoethanolamine-*N*-[methoxy(polyethyleneglycol)-2000] (DSPE-mPEG$_{2000}$) was acquired from Lipoid GmbH (Ludwigshafen, Germany). Pyrene P.A. (≥99.0%) was obtained from Sigma-Aldrich (Missouri, USA). 1,2-distearoyl-*sn*-glycero-3-phosphoethanolamine-*N*-[amine(polyethylenegliycol)-2000] (DSPE-PEG$_{2000}$-NH$_2$) was acquired from Avanti Polar Lipids, Inc (Alabama, USA). Diethylenetriaminepentaacetic (DTPA) dianhydride was from Sigma-Aldrich Co. (Missouri, USA). Pyridine e dimethyl sulfoxide (DMSO) were purchased from Labsynth (São Paulo, Brazil) and treated to remove residual water. Ethyl acetate was obtained from Tedia Company (Ohio, USA). Technetium–99 m was obtained from an alumina-based ^{99}Mo/^{99m}Tc generator from Institute of Energy and Nuclear Research (IPEN, São Paulo, Brazil). All other reagents were acquired from Sigma-Aldrich Co (Missouri, USA).

The murine mammary carcinoma cell line (4T1) was purchased from the American Type Culture Collection (ATCC, Rockville, USA). Female BALB/c mice were purchased from Bioterism Center of Federal University of Minas Gerais (CEBIO-UFMG), aging 6–8 weeks and weighing 20 ± 2 g. The mice were housed in cages in controlled environment to a temperature range of 25 ± 2 °C and a humidity range of 30–70% with a 12 h light-dark cycle and free access to food and water. All animals experiments were approved by Ethics Committee on Animal Use (CEUA) from UFMG, protocol number 205/2013.

2.2. Synthesis of DSPE-PEG$_{2000}$-DTPA

A solution of 25 mg of DSPE-PEG$_{2000}$-NH$_2$ prepared in 625 μL of DMSO was slowly added to 80 mg of DTPA dianhydride (excess of 25 mol equivalent) solubilized in a mixture of 2.5 mL dry DMSO: pyridine 7:3 (v/v) in a flask which was heated in an oil bath under constant stirring for 90 min at 100 °C. Ultrapure water was then added and the reaction was kept for 90 min at 100 °C then the solvents were evaporated. The residue was extracted successive times with ethyl acetate. Following evaporation, the content was re-suspended in

water and then purified by dialysis using a Spectrapore® membrane with a 1.0 kDa cut off, at room temperature for 36 h. Finally, the final product was lyophilized in a 24 h cycle and stored at −20 °C.

2.3. Characterization of DSPE-PEG$_{2000}$-DTPA

The structure of DSPE-PEG$_{2000}$-DTPA was characterized by MS, UV spectroscopy, and by FTIR spectroscopy using a Spectrum One FT-IR, (Pelkin Elmer, Massachusetts, USA) spectrometer. MS was performed on a matrix-assisted laser desorption/ionization time-of-flight (MALDI-ToF) Autoflex III spectrometer (Bruker Daltonics, Bremen, Germany). Sample (0.5 μL) were spotted onto an AnchorChip 600/384 (BrukerDaltonics, Bremen, Germany) target microtiter plate (MTP), mixed with a saturated solution of α-cyano-4-hydroxycinnamic acid (0.5 μL), and allowed to crystallize at room temperature. The MS spectra were acquired in the reflector/positive mode with external calibration, using Peptide Calibration Standard II as reference (BrukerDaltonics, Bremen, Germany). MS data analysis was performed by using the FlexAnalysis software (Bruker Daltonics).

2.4. Critical micelle concentration (CMC) determination

CMC of the DSPE-PEG$_{2000}$ was determined, at 25 °C, by spectrofluorimetry, using pyrene P.A. as fluorescent probe. Briefly, an aqueous dispersion of PEG$_{2000}$-DSPE was prepared and aliquots were transferred to the tubes containing 1 mg pyrene. Finally, the volume was adjusted to reach concentrations ranging from 10^{-4} and 10^{-6} mol L^{-1}. The mixtures were incubated overnight under stirring at room temperature. Free pyrene was removed by filtration through 0.22 μm polycarbonate membranes. The fluorescence of filtered samples was measured at the excitation wavelength of 339 nm and emission wavelength of 390 nm using a Cary eclipse fluorescence spectrometer (Varian, Inc. USA). CMC values correspond to the concentration of the polymer at which the sharp increase in pyrene fluorescence in solution was observed.

2.5. Preparation of DTPA-PM

DTPA-PMs were prepared using a solvent evaporation method [23,24]. Solutions of DSPE-mPEG$_{2000}$ and DSPE-PEG$_{2000}$-DTPA in chloroform, 95:5 (w/w) respectively, were transferred to a round bottom flask, at a 10 mmol L^{-1} final concentration. The solvent was completely removed under reduced pressure. Then, the thin film formed was hydrated with saline 0.9% (w/v), in a water bath at 40 °C for 5 min, followed by vortexing at 1000 rpm for 3 min. Lastly, the micelles were filtered in 0.22 μm polycarbonate membranes.

3. Physical and chemical characterization

3.1. Nanoparticle size

PMs size was analyzed by Dynamic Light Scattering (DLS) and Small Angle X-ray Scattering (SAXS). No previous procedures were required for both techniques in samples preparing. DLS analyses were performed in the Malvern Zetasizer NanoZS90 (Malvern Instruments Ltd, Malvern, UK), at 25 °C and a fixed angle of 90°. SAXS measurements were performed at the SAXS-1 beamline of the Brazilian Synchrotron Light Laboratory (LNLS, Campinas, Brazil) using a collimated beam with a fixed wavelength of 1.55 Å (8

keV). A two dimensional detector (Pilatus 300 K) was positioned at a distance of 0.5 m from the sample. The setup provides a q range that span from 0.05 to 2 nm^{-1}. Samples were placed in a temperature and vacuum controlled cell, made up with two mica windows separated by 1 mm, and immediately analyzed. The 2D images obtained from the detector were normalized and converted to line profiles I(q) versus q using the Fit2D (cake procedure) and OriginPro 8 software.

3.2. Zeta potential

The Zeta potential of the PM was analyzed by electrophoretic mobility determination using Malvern Zetasizer NanoZS90 (Malvern Instruments Ltd, Malvern, UK), at 25 °C and a fixed angle of 90°. For measurements, PMs were diluted 15-fold in saline 0.9% (w/v) previously filtered in 0.22 μm polycarbonate membranes.

3.3. Radiolabeling and radiochemical purity

250 μL of DTPA-PM were radiolabeled with ^{99m}Tc in the presence of 200 μg of stannous chloride, solubilized in HCl (0.25 mol L^{-1}), as reducing agent. The mixture (pH 7.0) was kept for 15 min at 25 °C. The radiolabeling yields were determined by thin layer chromatography (TLC-SG, Merck, Darmstadt, Germany) using acetone to determine $^{99m}TcO_4^-$. ^{99m}Tc-DTPA-PM were purified from $^{99m}TcO_2$ by a filtration through 0.22 μm polycarbonate membranes. Radioactivity was measured using a gamma counter (Wallac Wizard 1470–020 Gamma Counter; Perkin Elmer Inc., Waltham, MA, USA).

3.4. In vitro stability

TLC was used to estimate the stability of ^{99m}Tc-DTPA-PM in saline 0.9% (w/v) at room temperature (25 °C) and in mouse plasma at 37 °C. For saline, at specific times, the amount of TcO_4^- present in the radiolabeled MP was determined as mentioned previously. For plasma stability, 90 mL of labeled DTPA-PM solution was incubated, under agitation with 1.0 mL of mice fresh plasma. Radiochemical stability was determined from samples collected at 1, 2, 4, 6, 8 and 24 h after radiolabeling.

3.5. Blood clearance

An aliquot of 3.7 MBq of ^{99m}Tc-DTPA-PM was injected in the tail vein of healthy mice (n = 6) and blood samples were collected at 1, 5, 10, 15, 30, 45, 60, 120, 240, 360, 480 and 1440 min after administration. A small incision was made in the distal tail to facilitate rapid and reliable blood collection. Each sample was weighted, and the associated radioactivity was determined in an automatic scintillation apparatus. A standard dosage containing the same injected amount was counted simultaneously in a separate tube, which was defined as 100% radioactivity. The percentage of injected dose per gram (%ID/g) of blood was determined, and the data were plotted as function of time.

3.6. Cell culture

4T1 cells were cultured in Dulbecco's Modified Eagle medium (DMEM, Gibco, Waltham, MA, USA) containing 10% (v/v) fetal bovine serum, 100 IU/mL penicillin and 100 μg/mL streptomycin. Cells were kept in a humidified incubator with 5% CO2 atmosphere at 37 °C.

Cells were grown to confluence and then, harvested with 0.25% trypsin. After centrifugation at 500*g* for 5 min, cells were re-suspended in DMEM for inoculation into Balb/c mice.

3.7. 4T1 breast tumor model

For tumor implantation, an aliquot (100 μL) containing 2.5×10^6 4T1 cells was injected subcutaneously into the right flank of female BALB/c mice. Tumors were allowed to grow until it reached a volume of 100 mm^3 and then were used for biodistribution studies and scintigraphic images.

3.8. Biodistribution studies of ^{99m}Tc-DTPA-PM

The biodistribution studies were conducted using both healthy and 4T1 tumor-bearing mice. An aliquot of 3.7 MBq of ^{99m}Tc-DTPA-PM was injected intravenously into each animal, healthy (n = 5) and tumor-bearing mice (n = 6). After 1, 4, 8 and 24 h, mice were anesthetized with a mixture of xylazine (10 mg kg^{-1}) and ketamine (80 mg kg^{-1}). Whole heart, kidneys, blood, stomach, spleen, liver, thyroid, lungs, muscle and tumor (in the tumor groups) were removed, washed with distilled water, dried on filter paper, and placed in pre-weighed plastic test tubes. The radioactivity was measured using an automatic scintillation apparatus. A standard dosage containing the same injected amount was counted simultaneously in a separate tube, which was defined as 100% radioactivity. The results were expressed as%ID/g of tissue.

3.9. Scintigraphic images of ^{99m}Tc-DTPA-PM

Aliquots of 37 MBq of the ^{99m}Tc-DTPA-PM were injected intravenously into healthy and tumor-bearing mice (n = 6). Mice were anesthetized and horizontally placed under the collimator of a gamma camera (Mediso, Hungary) employing a low-energy high-resolution collimator. Images were acquired at 1, 4, 8 and 24 h post-injection using a 256 × 256 × 16 matrix size with a 20 % energy window set at 140 keV for a period of 300s.

3.10. Statistical analysis

All data are expressed as mean ± standard deviation (SD). Normality and homogeneity of variance was evaluated by the D'Agostino and Pearson, and Bartlett's tests, respectively. Variables without normal distribution were transformed when appropriate, by the equation: y = log (variable + 1). Data were tested using one-way analysis of variance (ANOVA) followed by Tukey's test. The 95% confidence interval was adopted and differences were considered significant when the p value was lower or equal to 0.05 ($p \leq 0.05$). All data were analyzed by GraphPad Prism version 5.00 software.

4. Results

4.1. Synthesis of DSPE-PEG_{2000}-DTPA

DTPA was covalently attached to DSPE-PEG_{2000}-NH_2 using an opening cyclic anhydride reaction, as schematically depicted on Fig. 1.

4.2. Chemical characterization of the DSPE-PEG$_{2000}$-DTPA

DSPE-PEG$_{2000}$-DTPA was obtained as a white powder with a 56% yield. UV spectra of the final product (DSPE-PEG$_{2000}$-DTPA) and the reactants (DTPA and DSPE-PEG$_{2000}$) were acquired in water solution at same concentration (2.6×10^{-6} mol%). UV absorption for DSPE-PEG$_{2000}$-DTPA was much higher than those obtained for DTPA and DSPE-PEG$_{2000}$ at the same wavelength (190 nm). FTIR was also performed for the final product and the two reactants (Fig. 2A). DTPA, DSPE-PEG$_{2000}$, and DSPE-PEG$_{2000}$-DTPA exhibited carbonyl stretching vibration bands at 1731 cm^{-1}, 1738 cm^{-1}, and 1728 cm^{-1}, respectively. Noteworthy was the broader carbonyl band for the product compared to DSPE-PEG$_{2000}$, which might be a consequence of several carbonyl bands from DTPA and DSPE-PEG$_{2000}$ merged on only one band.

Finally, MS was carried out to characterize and validate the final product. The mass spectra for DSPE-PEG$_{2000}$-DTPA and DSPE-PEG$_{2000}$ are presented in Fig. 2B. Due to the polymeric character of DSPE-PEG$_{2000}$-DTPA and DSPE-PEG$_{2000}$ several ion fragments were identified in both mass spectra. An increase in *m/z* (~375 Da) was observed for the DSPE-PEG$_{2000}$-DTPA compared to DSPE-PEG$_{2000}$. It is important to mention that the reason for such a mass increment might be the conjugation of DTPA to DSPE-PEG$_{2000}$, indicating the formation of the desired product DSPE-PEG$_{2000}$-DTPA. In addition, a peak of ion fragment at 3165 Da was also observed indicating DSPE-PEG$_{2000}$-DTPA formation.

4.3. CMC determination

The fluorescence intensity for eight different concentrations of DSPE-PEG$_{2000}$ in aqueous medium was evaluated. Then, a curve (fluorescence intensity vs concentration) was plotted (Fig. 3), and the CMC was determined as the concentration at the end of the first plateau of the fluorescence intensity. Therefore, the CMC was calculated as 1.8×10^{-5} mol L^{-1}.

4.4. Physical chemical characterization of the PM

PMs were found to have a mono-modal distribution by DLS with an average hydrodynamic diameter of 9.6 ± 0.6 nm (Fig. 4A) and zeta potential of −2.7 ± 1.1 mV. SAXS was also used to estimate the mean diameter of DSPE-PEG$_{2000}$ micelles. The measurement shown in Fig. 4B exhibit well defined local minima and is compatible with the scattering profile of nanoparticles from a mono-disperse micelle system. To directly retrieve this information (model-free data analysis) we used the equation proposed by SATO et al. [25], $D = 2\pi/q$, where “D” is the diameter of the micelle and the momentum transfer value q (scattering vector condition) corresponds to the position of the first intensity minimum observed [I(q)] (indicated by the black arrow of Fig. 4B). Such evaluation provides an average diameter of 10.0 ± 0.2 nm, corroborating the value obtained by DLS.

4.5. Radiochemical purity and stability

DTPA-MP was successfully labeled with ^{99m}Tc showing a radiochemical yield of 93.8 ± 2.1% (n = 5). Radiochemical impurities ($^{99m}TcO_4^-$ and $^{99m}TcO_2$) were quantified as 1.5 ± 2.0% and 4.3 ± 0.7%, respectively. However, the $^{99m}TcO_2$ was eliminated by the filtration process, which makes use of a 0.22 μm membrane. The radiolabeling exhibited a high in vitro stability (Fig. 5) within 24 h of incubation (n = 4) in saline. However, in mouse plasma,

a high stability was observed up to 8 h, but a slight reduction in the stability was verified 24 h post-incubation.

4.6. Blood clearance, biodistribution studies and scintigraphic images

The blood clearance profile of ^{99m}Tc-DTPA-PM after intravenous administration in healthy BALB/c female mice is shown in Fig. 6. ^{99m}Tc-DTPA-PM showed an area under curve (AUC) of 3515.7% ID/g min^{-1}. Blood levels declined in a biphasic manner with a α half-life of 65.5 min and a β half-life of 456.3 min.

Results of the biodistribution analysis conducted on healthy mice to estimate the location of the radiolabeled polymeric micelles are shown in Table 1. Biodistribution studies and scintigraphic images were also performed in 4T1 tumor-bearing mice (Figs. 7 and 8, respectively). A significantly high uptake in kidney, liver and spleen, was detected in all time frames evaluated, suggesting possible routes of elimination of the micelles. On the other hand, no significant uptake in the stomach or thyroid was observed, showing the absence of significant amounts of $^{99m}TcO_4^-$. For 4T1 tumor-bearing mice, tumor-to-muscle ratio from biodistribution and scintigraphic images were calculated for all the evaluated times (Table 2). Note that, tumor uptake was consistently higher than muscle uptake (Fig. 7–inset), indicating a preferential accumulation in tumor rather than in normal tissues. This can be directly visualized by the scintigraphic images of tumor-bearing animals (Fig. 8).

5. Discussion

Nanoparticles, including PMs, are ideal platforms for tumor delivery due to their ability to bypass biological limitations, thereby improving the targeting efficacy [26]. PMs might exhibit high payloads of therapeutic and diagnostic agents. Additionally, their surface can be functionalized with different varieties of ligands, such as chelating agents for ^{99m}Tc [27,28], making possible the early diagnosis, evaluation of the tumor burden and monitoring antitumor treatment progression [7,29]. Our group has previously described the use of DTPA onto the surface of silica nanoparticles as a means to achieve high radiolabeling yields[2]. By using this strategy, ^{99m}Tc is firmly attached to the nanoparticles, allowing the monitoring of nanoparticle fate in vivo. Therefore, in the present study, the DSPE-PEG$_{2000}$-DTPA complex was synthesized to allow the radiolabeling the micelles.

After synthesis and purification, DSPE-PEG$_{2000}$-DTPA was characterized by UV, FTIR, and MS. Carbonyl compounds have a $\pi \rightarrow \pi^*$ transition at about 188 nm [30], consequently, DTPA, DSPE-PEG$_{2000}$, and DSPE-PEG$_{2000}$-DTPA exhibit UV absorption at 190 nm. One must mention that the high UV absorption for DSPE-PEG$_{2000}$-DTPA is likely attributed to the presence of more carbonyl groups than due to the reactants. FTIR spectra for both lipids (DSPE-PEG$_{2000}$-DTPA and DSPE-PEG$_{2000}$) were similar; however by analyzing the carbonyl band for both molecules a broader band at 1700 cm^{-1} is observed (Fig. 2A), which might represent DTPA carboxylic acid groups along with carbonyl lipid band [31]. In order to validate the structural integrity, MS analysis was performed. As aforementioned, polymers such as PEG might present varying degrees of ethyleneglycol. Therefore, several peaks were found in the mass spectrum, Fig. 2B. For DSPE-PEG$_{2000}$-DTPA an average *m/z* increase of 375 Da (DTPA − H_2O) was clearly observed. This finding indicates that DSPE-

PEG_{2000}-DTPA was successfully synthesized and can be used for further radiolabeling studies.

PMs were properly obtained by solvent evaporation method using a mixture of DSPE-PEG_{2000}-DTPA and DSPE-PEG_{2000}. Micellar concentration was defined as 10 mmol L^{-1}, based on the calculated CMC value (1.8×10^{-5} mol L^{-1}). Previous studies reported CMC values of approximately 1.5×10^{-5} mol L^{-1} for DSPE-PEG_{2000} [32,39]. Determining CMC values of self-assembled systems (i.e. micelles) is particularly important to evaluate their potential for biological applications. A serious issue faced using this delivery platform is the disruption after dilution in a larger volume, such as bloodstream dilution. Consequently, copolymers with high CMC values might dissociate and release their content before reaching the targeting tissue [33,34]. Therefore, CMC values found in this study suggest that PM will remain stable even after diluting in a blood volume of a normal 70 kg-human (approximately 5 L). By analyzing the zeta potential of PM we found that, although DSPE is a negatively charged lipid, the presence of PEG promotes a fixed aqueous layer at the surface of micelles that diminish the electrophoretic mobility, resulting in a neutral zeta potential. Furthermore, the use of hydrophilic polymers, including PEG, contributes to the stability of micelles preventing aggregation by the steric repulsion mechanism [35].

The PM were radiolabeled with ^{99m}Tc through a standard and extensively employed procedure for labeling DTPA, which involves the use of $Na^{99m}TcO_4^-$ in presence of $SnCl_2$ as reducing agent [2,36]. The radiochemical yield of the ^{99m}Tc-DTPA-PM was determined by quantifying $^{99m}TcO_4^-$ and $^{99m}TcO_2$. To determine the percentage of the $^{99m}TcO_4^-$, TLC was used. $^{99m}TcO_4^-$ migrates to the top of silica gel plaques, while the ^{99m}Tc-DTPA-PM remains at the bottom. $^{99m}TcO_2$ was quantified and eliminated from the ^{99m}Tc-DTPA-PM dispersion by filtration through a 0.22 μm membrane. Radiochemical purity higher than 90% was achieved. This is essential for in vivo studies, such as biodistribution and scintigraphic Images [37]. ^{99m}Tc-DTPA-PM showed high stability in the presence of saline or plasma for upwards of 8 h. However, at 24 h post-incubation a decrease of approximately 20% of radiolabeling stability was observed. This is a critical aspect of radiolabeled nanoparticles, since a low stability results in isotope detachment from micelles and the biodistribution will no longer reflect the nanoparticle fate [21,37]. It is important to underscore that the scintigraphic images did not show thyroid or stomach uptake even at 24 h post-injection. This finding indicates that the slight reduction in stability does not compromise in vivo studies.

Blood clearance of ^{99m}Tc-DTPA-PM showed biphasic decay, where initially a fraction of micelles shrink due to osmotic forces and may undergo an initial burst-release effect upon entering the blood. Subsequently, the majority of micelles remain in the bloodstream, which is consistent with the longer β half-life [38,39]. β half-life of ^{99m}Tc-DTPA-PM is close to optimal half-life (2–6 h) for imaging probes, allowing accumulation at the targeted site, clearance from non-targeted areas and data collection [40].

As expected, biodistribution and imaging studies on healthy and tumor-bearing mice, showed high uptake in liver and spleen throughout the experiments. Such increased uptake and retention might be attributed to the activation of the Mononuclear Phagocyte System

[14,41]. In addition, we observed a moderate uptake in kidneys suggesting that renal clearance partially contributes to the elimination of micelles and corroborates the biphasic decay pattern. These data are consistent with elimination of particles smaller than 5 nm and monomers after micelles disruption [38].

Tumor-to-muscle ratios increased over time, suggesting that accumulation is time-dependent. This is consistent with an increased blood-circulation time that can lead to a higher tumor accumulation due to large amount of passages through the tumor region [13,40,42]. Importantly, ratios (biodistribution and imaging) were higher than 2.0 for all evaluated timeframes. It has been established that radiotracers showing tumor-to-muscle ratio higher than 1.5 (50% more uptake in the targeting tissue) can be considered as promising imaging probes for tumor identification [43,44].

Herein we proposed a new strategy for radiolabeling micelles in a straightforward method. Other methodologies reported in the literature [45,46], for Indium-111 complexation, show some disadvantages such as lengthy and laborious of labeling procedure and higher radiation exposure. Our ^{99m}Tc labeling protocol enables an easy, fast and reliable alternative to prepare radiolabeled micelles for imaging proposes. Furthermore, the described system may also represent a promising platform in cancer therapy, since it presents a great potential for carrying and delivering hydrophobic drugs, in special for fenestrated tissues, such as solid tumors. Moreover, other contrast agents, such as Gadolinium (for magnetic resonance imaging [47]) can be easily associated in the DTPA portion of the PM developed. Another possibility for the proposed system is its functionalization for active targeting purposes for specific tumors [48]. In this way, our platform enables multifunctional micelles associating diagnostic and therapeutic capabilities for both target-specific diagnosis and treatment of cancer.

6. Conclusion

DSPE-PEG$_{2000}$-DTPA was successfully synthesized, and allowed the development of ^{99m}Tc-DTPA-PM with high radiolabeling yields and high stability. In vivo studies showed a long circulation time and preferential tumor targeting, indicating that this system might be a promising platform for simultaneous delivery of therapeutic agents and diagnostic probes allowing for treating and monitoring the stage of the disease using a single formulation.

Acknowledgments

The authors would like to thank FAPEMIG, CNPq and LNLS (Campinas, Brazil) for their financial support. Caroline M.R. Oda would like to thank CAPES for supporting her with a scholarship.

References

1. Svenson S. What nanomedicine in the clinic right now really forms nanoparticles. WIREs Nanomed. Nanobiotechnol. 2014; 6:125–135.
2. de Barros ALB, Ferraz KSO, Dantas TCS, Andrade GF, Cardoso VN, de Sousa EMB. Synthesis, characterization, and biodistribution studies of 99mTc-labeled SBA-16 mesoporous silica nanoparticles. Mater. Sci. Eng. C: Mater. Biol. Appl. 2015; 56:181–188. [PubMed: 26249579]

3. Cheng S-H, Yu D, Tsai H-M, Morshed RA, Kanojia D, Lo L-W, Leoni L, Govind Y, Zhang L, Aboody KS, Lesniak MS, Chen C-T, Balyasnikova E. Dynamic in vivo SPECT imaging of neural stem cells functionalized with radiolabeled nanoparticles for tracking of glioblastoma. J. Nucl. Med. 2016; 57:279–284. [PubMed: 26564318]
4. Laan AC, Santini C, Jennings L, Jong M, Bernsen MR, Denkova AG. Radiolabeling polymeric micelles for in vivo evaluation: a novel, fast, and facile method. EJNMMI Res. 2016; 6:1–10. [PubMed: 26728358]
5. Lepareur N, Costa LLE, Bocqué M, Blondelle C, Ruello C, Desjulets M, Noiret N, Cammas-Marion M. Development of biocompatible and functional polymeric nanoparticles for site-specific delivery of radionuclides. Front. Med. 2015; 2:1–9.
7. Xing Y, Zhao J, Conti PS, Chen K. Radiolabeled nanoparticles for multimodality tumor imaging. Theranostics. 2014; 4:290–306. [PubMed: 24505237]
8. Croy S, Kwon GS. Polymeric micelles for drug delivery. Curr. Pharm. Des. 2006; 12:4669–4684. [PubMed: 17168771]
9. Oerlemans C, Bult W, Bos M, Storm G, Nijsen JFW, Hennink WE. Polymeric micelles in anticancer therapy: targeting: imaging and triggered release. Pharm. Res. 2010; 27:2569–2589. [PubMed: 20725771]
10. Yokoyama M. Polymeric micelles as drug carriers: their lights and shadows. J. Drug Target. 2014; 22:576–583. [PubMed: 25012065]
11. Gill KK, Kaddoumi A, Nazzal S. PEG–lipid micelles as drug carriers: physiochemical attributes, formulation principles and biological implication. J. Drug Target. 2015; 23:222–231. [PubMed: 25547369]
12. Musacchio T, Laquintana V, Latrofa A, Trapani G, Torchilin VP. PEG-PE micelles loaded with paclitaxel and surface-modified by a PBR-ligand: synergistic anticancer effect. Mol. Pharm. 2009; 6:468–479. [PubMed: 19718800]
13. Gao H, Liu J, Yang C, Cheng T, Chu L, Xu H, Meng A, Fan S, Shi L, Liu J. The impact of PEGylation patterns on the in vivo biodistribution of mixed micelles. Int. J. Nanomed. 2013; 8:4229–4246.
14. Kolate A, Baradia D, Patil S, Vhora I, Kore G, Misra A. PEG −a versatile conjugating ligand for drugs and drug delivery systems. J. Controlled Release. 2014; 192:67–81.
15. Torchilin VP. Micellar nanocarriers: pharmaceutical perspectives. Pharm. Res. 2006; 24:1–16. [PubMed: 17109211]
16. de Barros ALB, Tsourkas A, Saboury B, Cardoso VN, Alavi A. Emerging role of radiolabeled nanoparticles as an effective diagnostic technique. EJNMMI Res. 2012; 2:1–15. [PubMed: 22251281]
17. Stacy MR, Maxfiel MW, Sinusas AJ. Targeted molecular imaging of angiogenesis in PET and SPECT: A review. Yale J. Biol. Med. 2012; 85:75–86. [PubMed: 22461745]
18. Hong H, Zhang Y, Sun J, Cai W. Molecular imaging and therapy of cancer with radiolabeled nanoparticles. Nano Today. 2009; 4:399–413. [PubMed: 20161038]
19. de Barros ALB, Andrade SF, Filho JDS, Cardoso VN, Alves RJ. Radiolabeling of low molecular weight D-galactose-based glycodendrimer with technetium-99 m and biodistribution studies. J. Radioanal. Nucl. Chem. 2013; 298:605–659.
20. Varshney R, Sethi SK, Hazari PP, Chuttani K, Soni S, Milton MD, Mishra AK. Synthesis of[DTPA-bis(D-ser)] chelate (DBDSC): An approach for the design of SPECT radiopharmaceuticals based on technetium. Curr. Radiopharm. 2012; 5:348–355. [PubMed: 22642421]
21. Zhu X, Li J, Hong Y, Kimura RH, Ma X, Liu H, Qin C, Hu X, Hayes TR, Benny P, Gambhir SS, Cheng Z. 99mTc-labeled cystine knot peptide targeting integrin αvβ6 for tumor SPECT imaging. Mol. Pharm. 2014; 11:1208–1217. [PubMed: 24524409]
22. Hazari PP, Shukla G, Goel V, Chuttani K, Kumar N, Sharma R, Mishra AK. Synthesis of specific SPECT-radiopharmaceutical for tumor imaging based on methionine: 99mTc-DTPA-bis(methionine). Bioconjug. Chem. 2010; 21:229–239. [PubMed: 20108938]
23. Sawant RR, Torchilin VP. Multifunctionality of lipid-core micelles for drug delivery and tumour targeting. Mol. Membr. Biol. 2010; 7:232–246.

24. Wang T, Petrenko VA, Torchilin VP. Paclitaxel-loaded polymeric micelles modified with MCF-7 cell-specific phage protein: enhanced binding to target cancer cells and increased cytotoxicity. Mol. Pharm. 2010; 7:1007–1014. [PubMed: 20518562]
25. Sato T, Sakai H, Sou K, Buchner R, Tsuchida E. Poly(ethylene glycol)-conjugated phospholipids in aqueous micellar solutions: hydration, static structure, and interparticle interactions. J. Phys. Chem. Biol. 2007; 111:1393–1401.
26. Bertrand N, Wu J, Xu X, Kamaly N, Farokhzad OC. Cancer nanotechnology: the impact of passive and active targeting in the era of modern cancer biology. Adv. Drug Deliv. Rev. 2013; 66:2–25. [PubMed: 24270007]
27. Torchilin VP. Tageted pharmaceutical nanocarriers for cancer therapy and imaging. AAPS J. 2007; 9:129–147.
28. Mirshojaei SF, Ahmadi A, Morales-Avila E, Ortiz-Reynoso M, Reyes-Perez H. Radiolabelled nanoparticles: novel classification of radiopharmaceuticals for molecular imaging of cancer. J. Drug Target. 2016; 24:91–101. [PubMed: 26061297]
29. Kumar R, Kulkarni A, Nageska DK, Sridhar S. In vitro evaluation of theranostic polymeric micelles for imaging and drug delivery in cancer. Theranostics. 2012; 2:714–722. [PubMed: 22896773]
30. Pavia, DL., Lampman, GM., Kriz, GS., Vyvyan, JR. Introduction to Spectroscopy. 4. Vol. 2. Brooks/Cole Cengage Learning; Belmont, CA: 2009. Infrared spectroscopy; p. 15-104.
31. Pavia, DL., Lampman, GM., Kriz, GS., Vyvyan, JR. Introduction to Spectroscopy. 4. Vol. 7. Brooks/Cole Cengage Learning; Belmont, CA: 2009. Ultraviolet spectroscopy; p. 381-417.
32. Sawant RR, Sawant RM, Torchilin VP. Mixed PEG-PE/vitamin E tumor-targeted immunomicelles as carriers for poorly soluble anti-cancer drugs: improved drug solubilization and enhanced in vitro cytotoxicity. Eur. J. Pharm. Biopharm. 2008; 70:51–57. [PubMed: 18583114]
33. Grallert SRM, Rangel-Yangui CO, Pasqualoto KFM, Tavares LC. Polymeric micelles and molecular modeling applied to the development of radiopharmaceuticals. Braz. J. Pharm. Sci. 2012; 48:1–16.
34. Shuai X, Ai H, Nasongkla N, Kim S, Gao J. Micellar carriers based on block copolymers of poly(ε-caprolactone) and poly(ethylene glycol) for doxorubicin delivery. J. Controlled Release. 2004; 98:415–426.
35. Hu Y, Xie J, Tong WY, Wang C. Effect of PEG conformation and particle size on the cellular uptake effiency of nanoparticles with the HepG2 cells. J. Controlled Release. 2007; 118:7–17.
36. Aldenhoff Y, van Kroonenburgh MJPG, Koole LH. Preparation: characterization and radiolabeling of a new amphiphilic derivative of DTPA. Nucl. Med. Biol. 1996; 23:653–656. [PubMed: 9044688]
37. Saha GB. Radiopharmaceuticals and methods of radiolabeling. Fundamentals of Nuclear Pharmacy (6). 2010; 6:83–113.
38. Pearson RM, Juettner VV, Hong S. Biomolecular corona on nanoparticles: a survey of recent literature and its implications in targeted drug delivery. Front. Chem. 2014; 2:1–7.
39. Sun Q, Radosz M, Shen Y. Challenges in design of translational nanocarriers. J. Controlled Release. 2012; 164:156–169.
40. Jokerst JV, Lobovkina T, Zare RN, Gambhir SS. Nanoparticle PEGylation for imaging and therapy. Nanomedicine. 2011; 6:715–728. [PubMed: 21718180]
41. Kiessling F, Mertens MR, Grimm J, Lammers T. Nanoparticles for imaging. Top or flop. Radiology. 2014; 273:10–28. [PubMed: 25247562]
42. He X, Li L, Su H, Zhou D, Song H, Wang L, Jiang X. Poly(ethylene glycol)-block-poly((-caprolactone) and phospholipid-based stealth nanoparticles with enhanced therapeutic efficacy on murine breast cancer by improved intracellular drug delivery. Int. J. Nanomed. 2015; 10:1791–1804.
43. de Barros ALB, Cardoso VN, Mota LG, Alves RJ. Synthesis and biodistribution studies of carbohydrate derivatives radiolabeled with technetium-99m. Bioorg. Med. Chem. Lett. 2010; 20:315–317. [PubMed: 19926278]
44. Phillips WT. Delivery of gamma-imaging agents by liposomes. Adv. Drug Deliv. Rev. 1999; 37:13–32. [PubMed: 10837724]

45. Kaida S, Cabral H, Kumagai M, Kishimura A, Terada Y, Sekino M, Aoki I, Nishiyama N, Tani T, Kataoka K. Visible drug delivery by supramolecular nanocarriers directing to single-platformed diagnosis and therapy of pancreatic tumor model. Cancer Res. 2010; 70:7031–7041. [PubMed: 20685894]

46. Laan AC, Santini C, Jennings L, de Jong M, Bernsen MR, Denkova AG. Radiolabeling polymeric micelles for in vivo evaluation: a novel fast and facile method. EJNMMI Res. 2016; 6:1–10. [PubMed: 26728358]

47. Wang T, Yang S, Mei LA, Pamar CK, Gillespie JW, Praveen KP, Petrenko VA, Torchilin VP. Paclitaxel-loaded PEG-PE-based micellas nanopreparations targeted with tumor-specific landscape phage fusion protein enhance apoptosis and efficiently reduce tumors. Mol. Cancer Ther. 2014; 13:2864–2875. [PubMed: 25239936]

48. Lukyanov AN, Gao Z, Mazzola L, Torchilin VP. Polyethylene glycol-diacyllipid micelles demonstrate increased accumulation in subcutaneous tumors in mice. Pharm. Res. 2002; 19:1424–1429. [PubMed: 12425458]

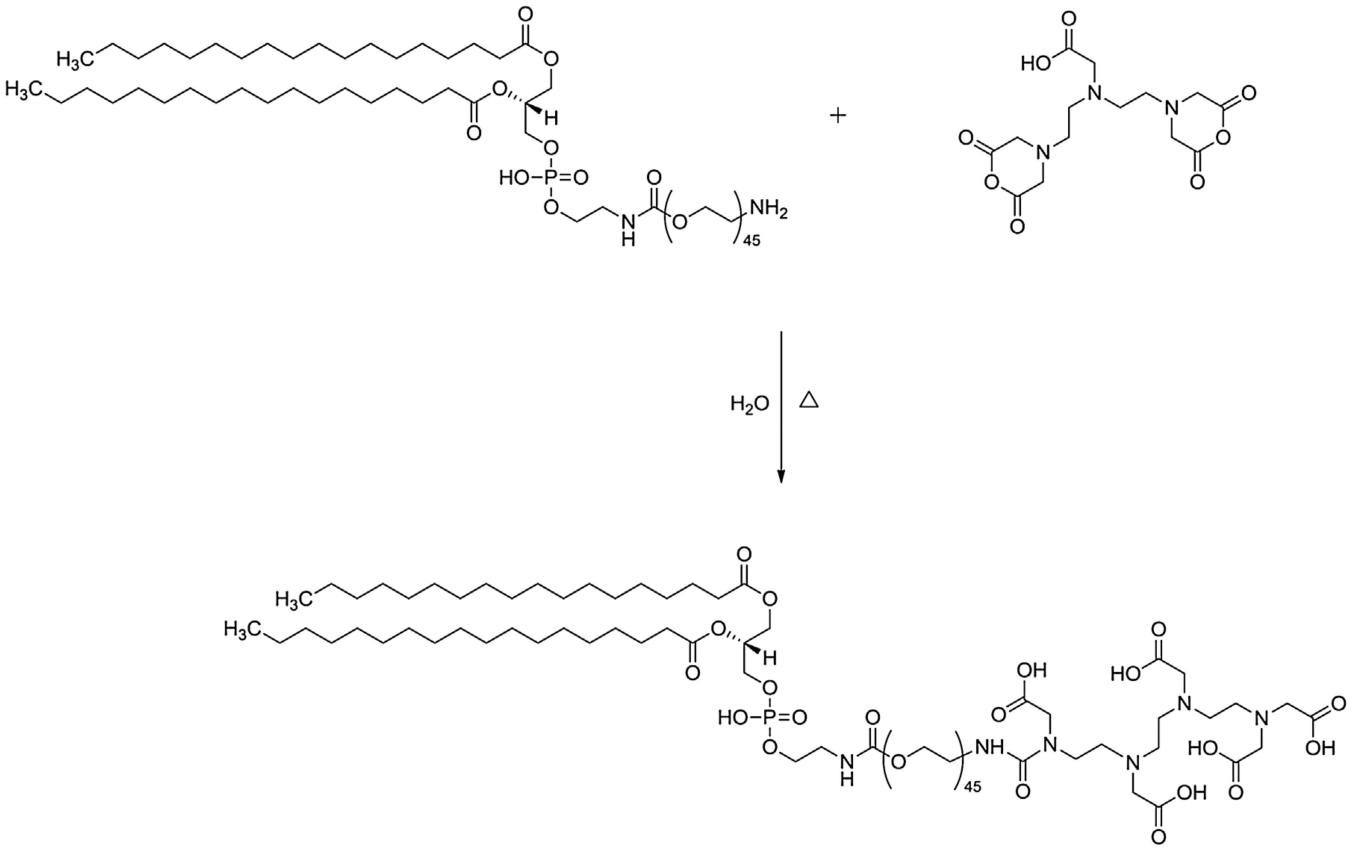

Fig. 1.
Representative scheme of the synthesis of DSPE-PEG$_{2000}$-DTPA.

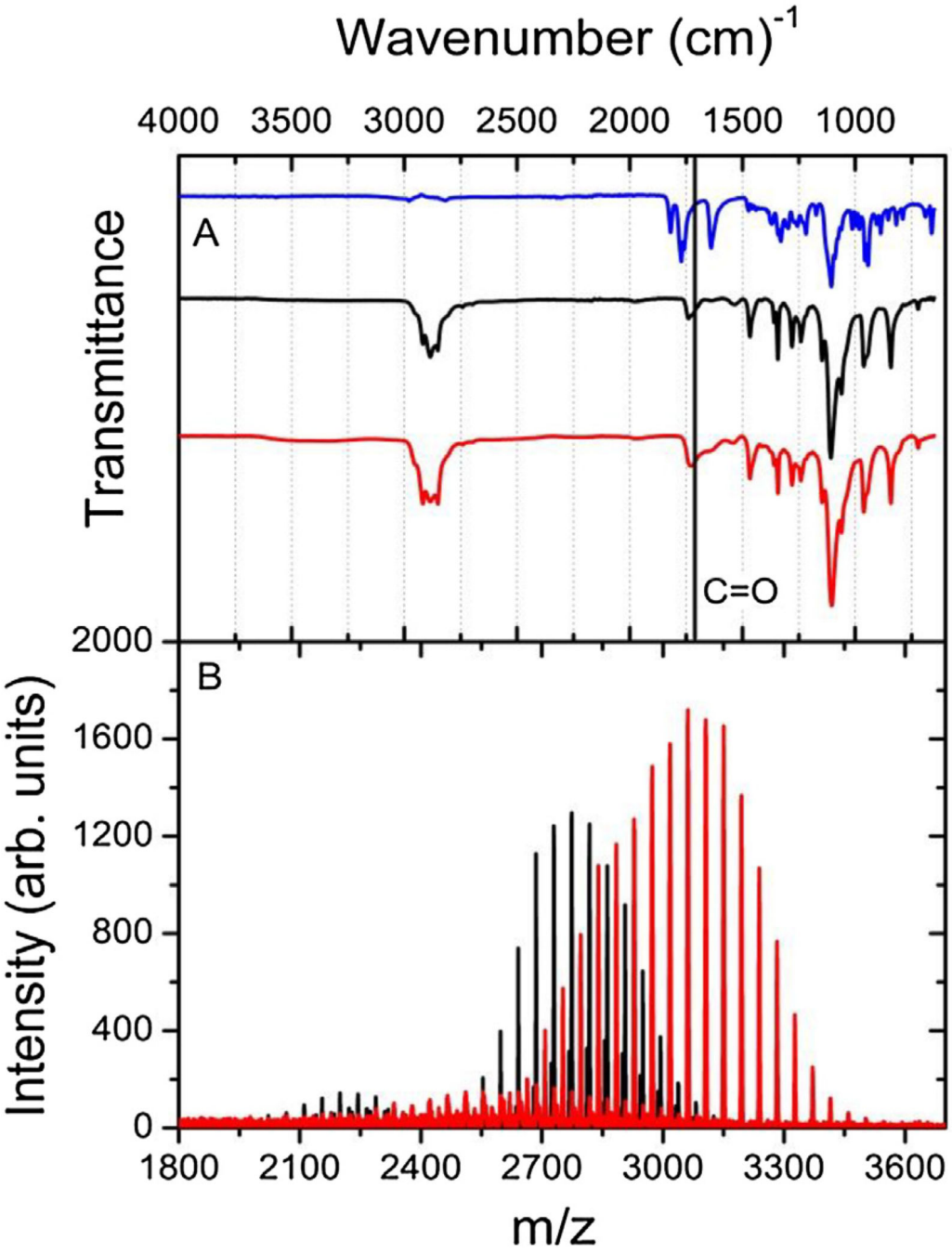

Fig. 2.

(A) FTIR spectra of DTPA (blue), DSPE −PEG_{2000}-NH_2 (black), and DSPE-PEG_{2000}-DTPA (red). (B) Mass spectrum of DSPE −PEG_{2000}-NH_2 (black), and DSPE-PEG_{2000}-DTPA (red).

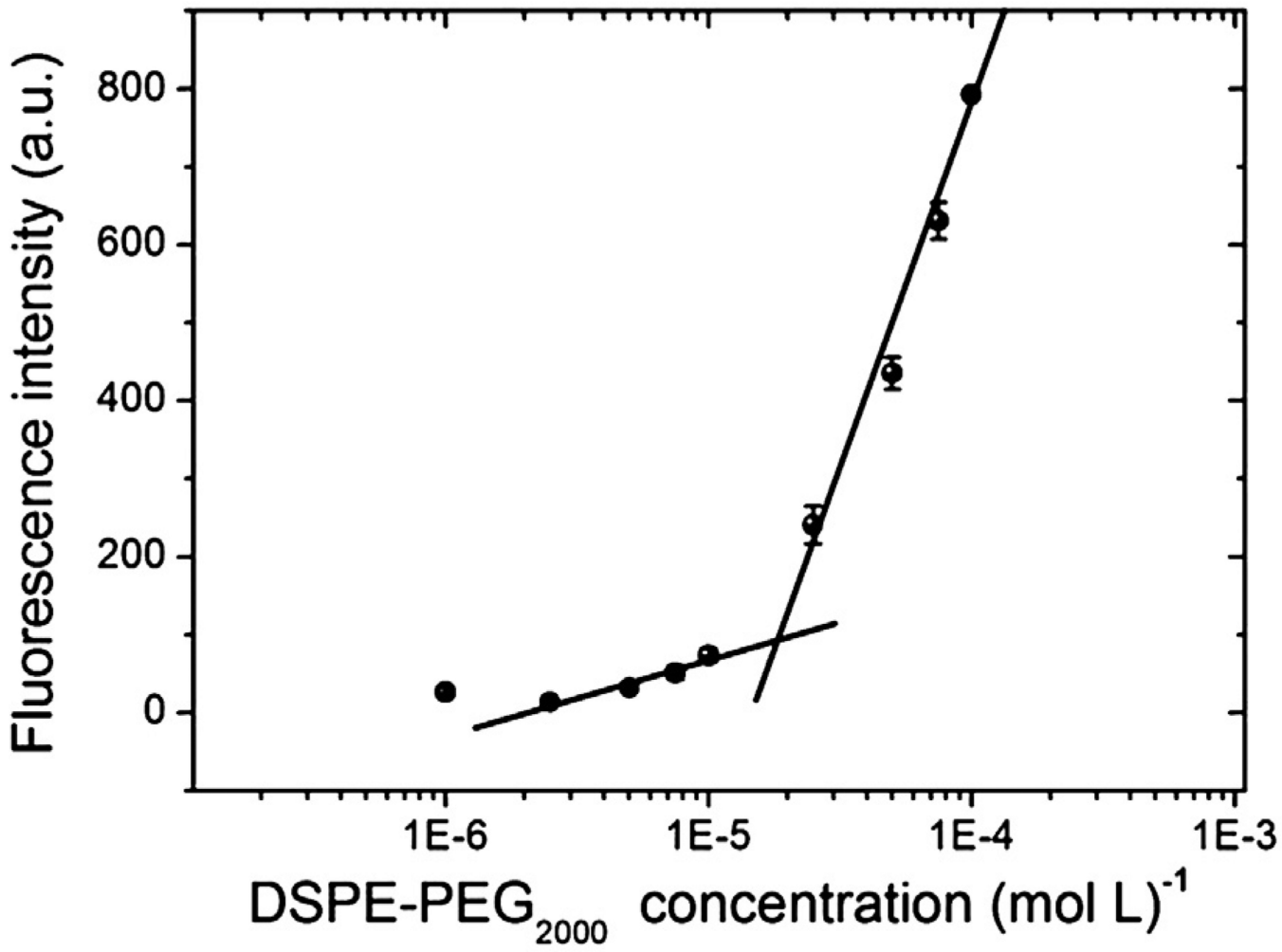

Fig. 3.

Pyrene fluorescence intensity versus DSPE-PEG_{2000} concentration for determination of CMC. The data expressed as mean ± standard deviation of the mean (n = 3).

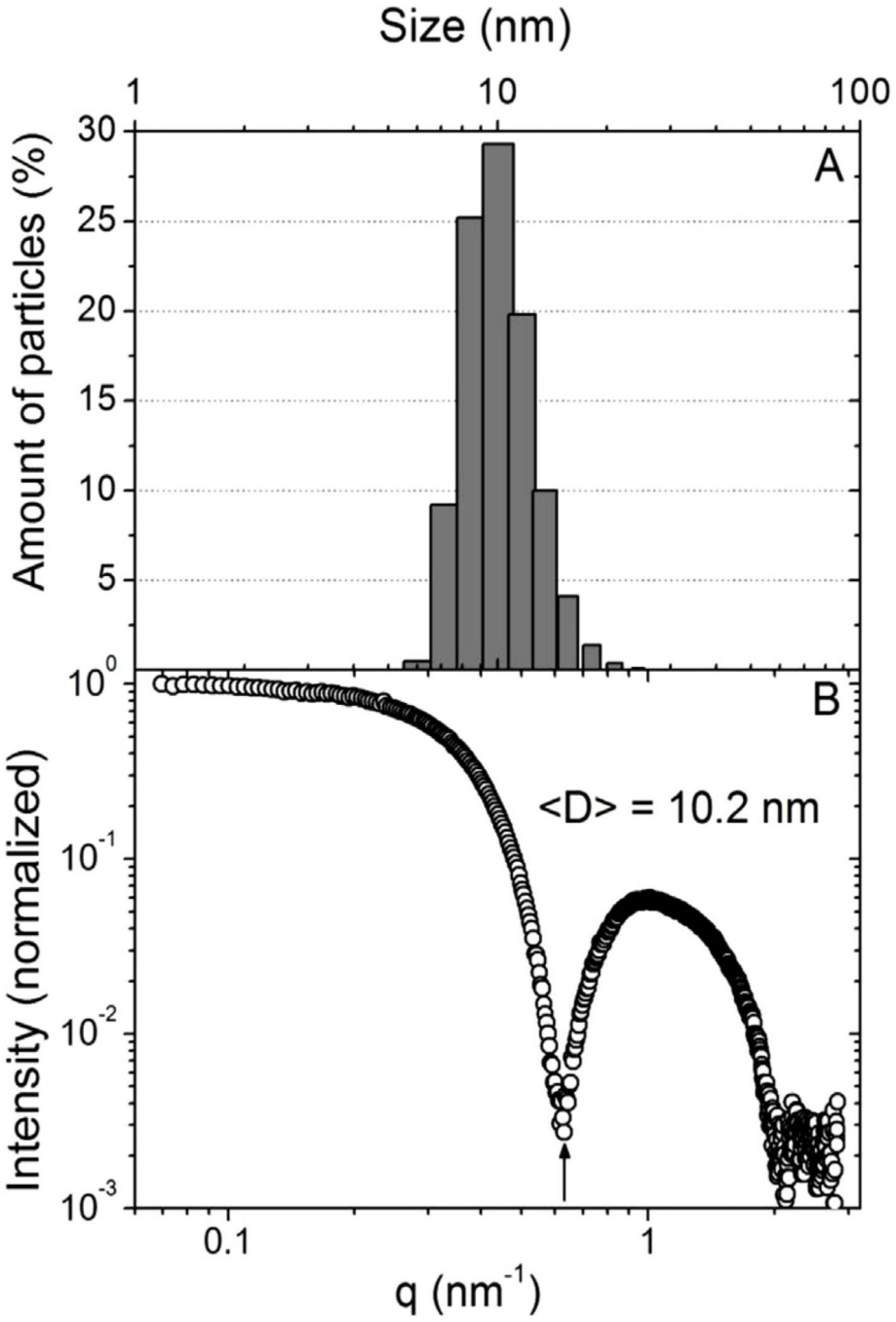

Fig. 4.
(A) Size distribution of PM according DLS technique; (B) SAXS pattern of PM.

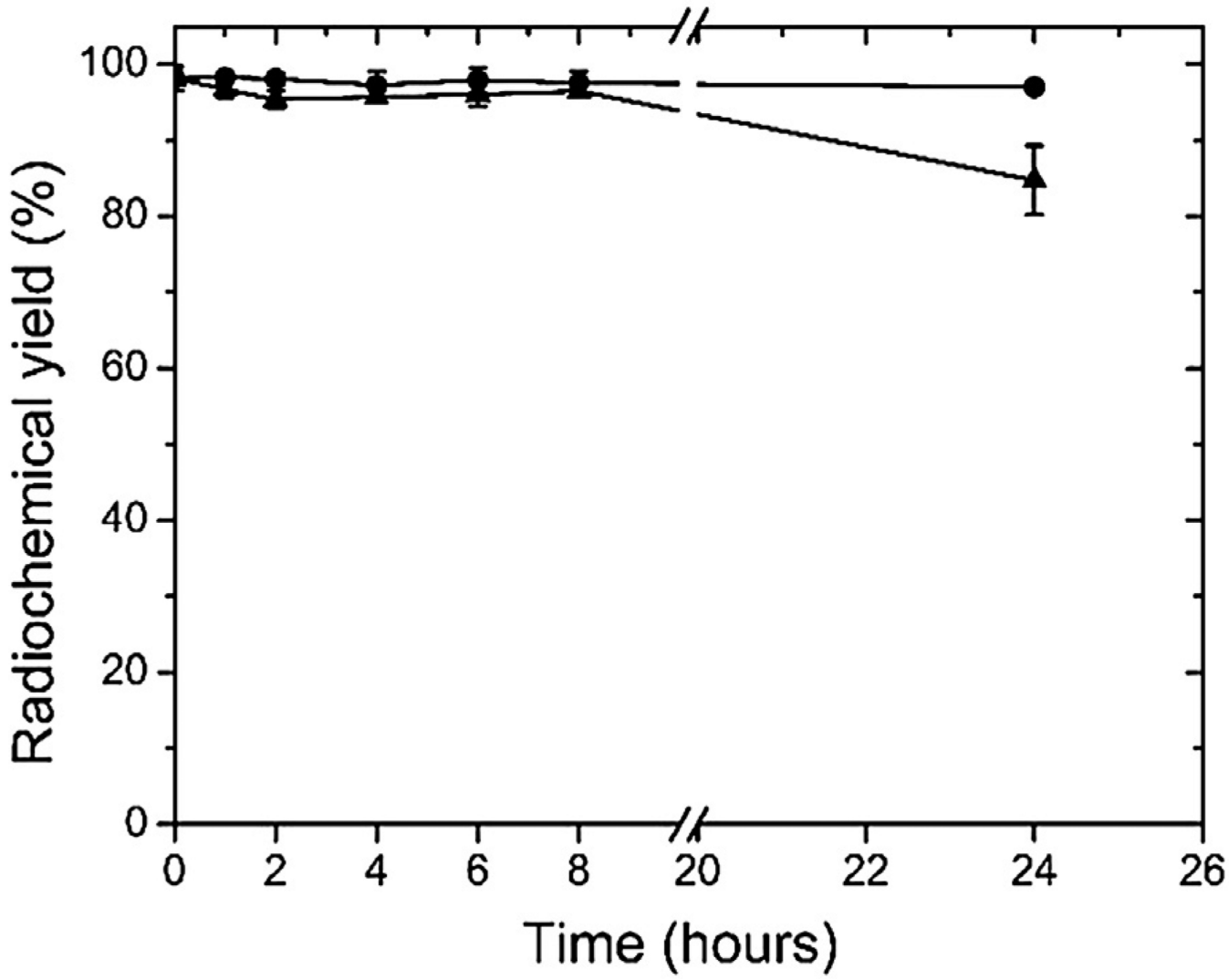

Fig. 5.

In vitro stability of radiolabeling of DTPA-PM determined in saline 0.9% (circles) at room temperature (25 °C) and in presence of mice plasma (triangles) at 37 °C. Data expressed as mean ± standard deviation of the mean (n = 4).

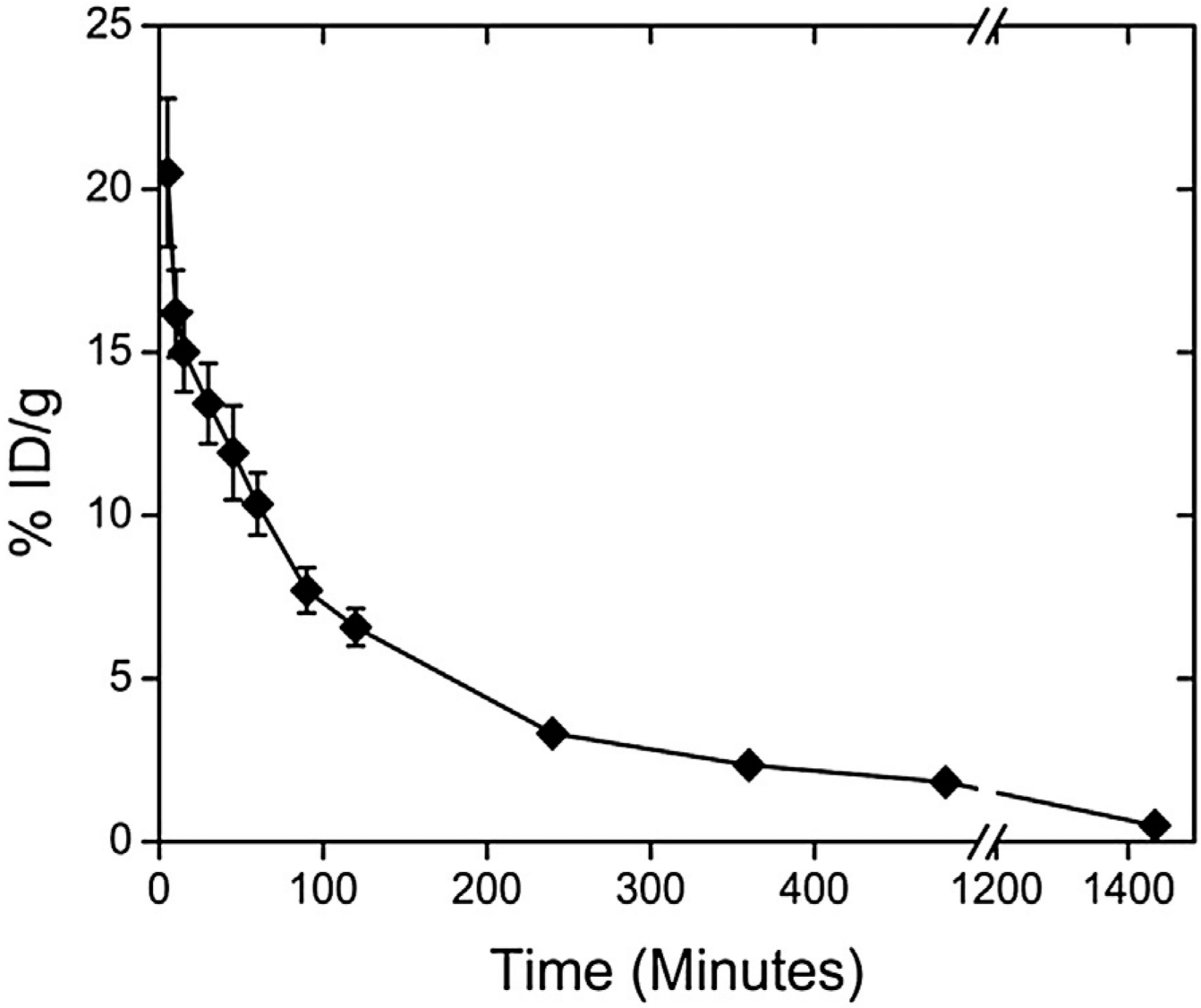

Fig. 6.

Blood clearance profile of ^{99m}Tc-DTPA-PM after intravenous administration in healthy mice. The data are expressed as mean percentage of the injected dose ± the standard deviation of the mean (n = 6).

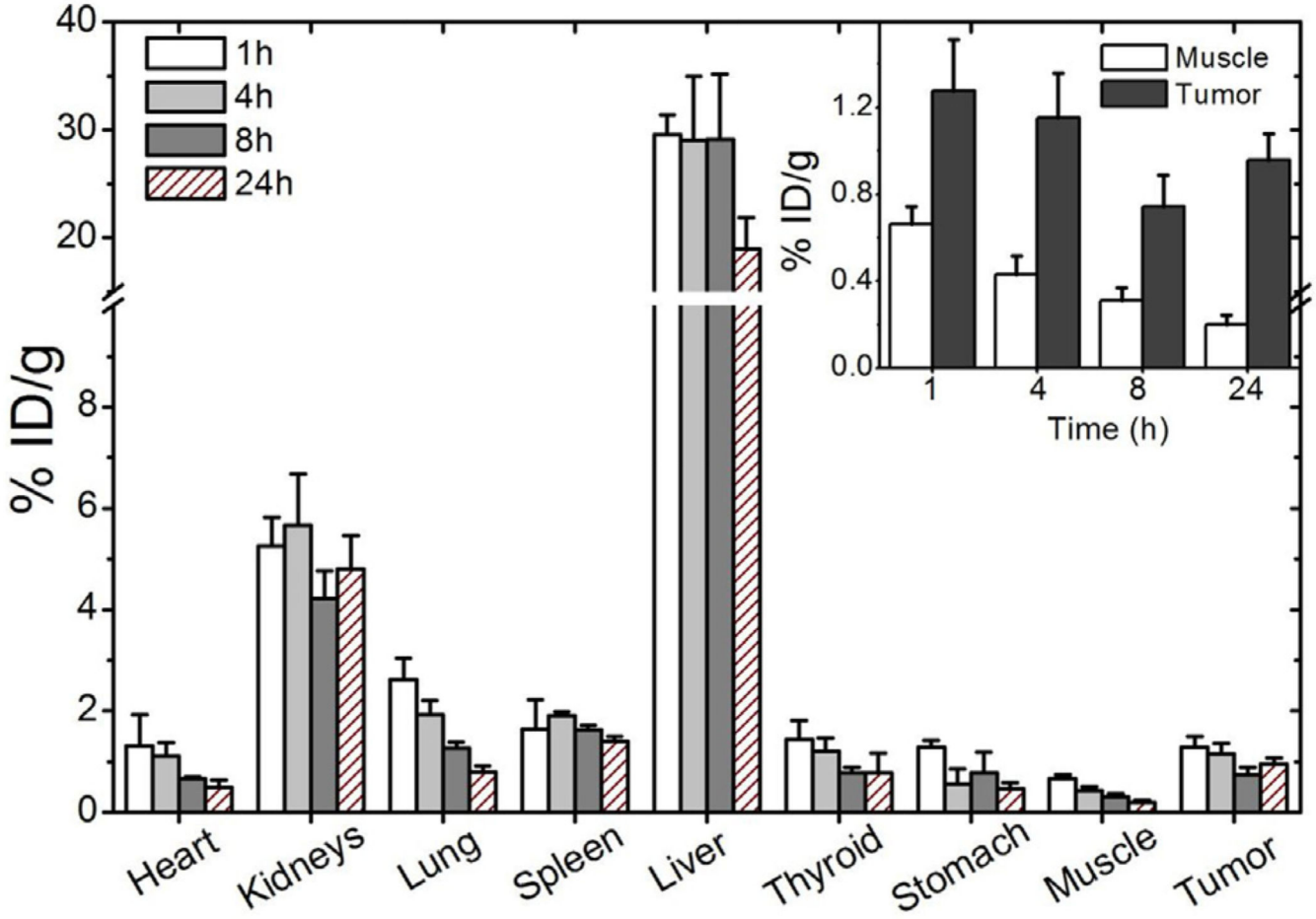

Fig. 7.

Biodistribution profile at 1, 4, 8, and 24 h after ^{99m}Tc-DTPA-PM administration in 4T1 tumor-bearing mice (n = 5). Inset: tumor and muscle uptake at 1, 4, 8 and 24 h after injection. All data are expressed as the mean percentage of the injected dose of ^{99m}Tc-DTPA-PM per gram of tissue ± the standard deviation of the mean (n = 5).

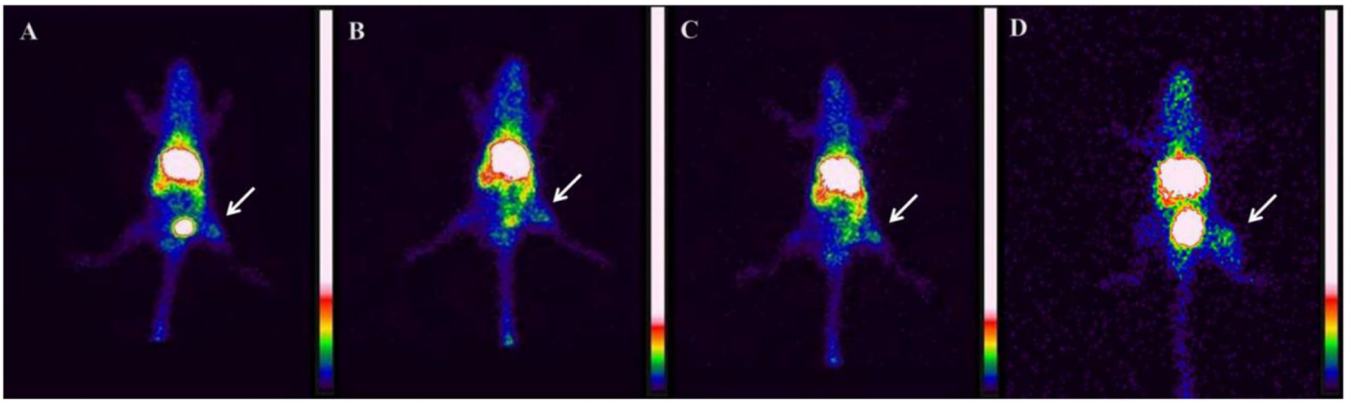

Fig. 8.

Scintigraphic images at 1 (A), 4 (B), 8 (C), and 24 h (D) after ^{99m}Tc-DTPA-PM administration in 4T1 tumor-bearing mice (n = 5). Arrows indicate tumor area.

Table 1

Biodistribution of ^{99m}Tc-DTPA-PM in healthy mice (% ID/g).

	Group			
Tissue	**1 h**	**4 h**	**8 h**	**24 h**
Heart	2.4 ± 0.3	1.1 ± 0.1	0.5 ± 0.1	0.3 ± 0.1
Kidneys	9.8 ± 1.2	8.1 ± 1.2	7.6 ± 1.6	9.4 ± 1.4
Stomach	3.4 ± 1.4	0.7 ± 0.1	0.5 ± 0.2	0.3 ± 0.2
Spleen	10.9 ± 2.1	6.7 ± 1.2	6.7 ± 1.4	10.9 ± 2.9
Liver	33.9 ± 2.9	21.8 ± 5.0	31.1 ± 3.0	34.2 ± 6.6
Thyroid	2.2 ± 0.3	1.1 ± 0.2	0.6 ± 0.2	0.7 ± 0.3
Lung	3.7 ± 0.5	1.8 ± 0.2	1.1 ± 0.1	0.6 ± 0.1
Muscle	1.2 ± 0.5	0.4 ± 0.1	0.4 ± 0.2	0.2 ± 0.03

All data are expressed as the mean percentage of the injected dose of ^{99m}Tc-DTPA-PM per gram of tissue ± the standard deviation of the mean (n = 5).

Table 2

Tumor-to-muscle ratios, from biodistribution and scintigraphic images, achieved after intravenous injection of ^{99m}Tc-DTPA-PM in 4T1 tumor-bearing mice.

	Time (h)			
	1	**4**	**8**	**24**
Scintigraphic images	2.4 ± 0.2	2.8 ± 0.3	3.3 ± 0.4[a]	2.8 ± 0.3
Biodistribution	1.9 ± 0.2[b]	2.7 ± 0.4[b]	2.5 ± 0.8[b]	5.0 ± 1.3

Data are expressed as the mean ± the standard deviation of the mean (n = 6).

[a]Represents significant difference when compared with tumor-to-muscle ratio at 1 h post-injection.

[b]Represents significant difference when compared with tumor-to-muscle ratio at 24 h post-injection.